Computational Mechanics manuscript No.
(will be inserted by the editor)

A finite strain framework for the simulation of polymer curing. Part II: viscoelasticity and shrinkage

M. Hossain · G. Possart · P. Steinmann

Received: date / Accepted: date

Abstract A phenomenologically inspired, *elastic* finite strain framework to simulate the curing of polymers has been developed and discussed in the first part [1] of this work. The present contribution provides an extension of the previous simulation concept towards the consideration of *viscoelastic* effects and the phenomenon of *curing shrinkage*.
The presented approach is particularly independent from the type of the free energy density, i.e. any phenomenologically or micromechanically based viscoelastic polymer model can be utilised. For both cases the same representatives that have been used for the elastic curing models, i.e. the Neo-Hookean model and the 21-chain microsphere model, are reviewed and extended accordingly. The governing equations are derived as well as the corresponding tangent operators necessary for the numerical implementation within the finite element method. Furthermore, we investigate two different approaches – a shrinkage strain function and a multiplicative decomposition of the deformation gradient – to capture the phenomenon of curing shrinkage, i.e. the volume reduction induced by the polymerisation reaction which may lead to significant residual stresses and strains in the fully cured material. Some representative numerical examples conclude this work and prove the capability of our approach to correctly capture inelastic behaviour and shrinkage effects in polymers undergoing curing processes.

M. Hossain, G. Possart, P. Steinmann
Chair of Applied Mechanics, University of Erlangen-Nuremberg,
Egerlandstrasse 5, 91058 Erlangen, Germany
Tel.: +49-9131-85-28502
Fax: +49-9131-85-28503
E-mail: mokarram.hossain@ltm.uni-erlangen.de
E-mail: gunnar.possart@ltm.uni-erlangen.de
E-mail: paul.steinmann@ltm.uni-erlangen.de

Keywords polymers · curing · finite strains · viscoelasticity · shrinkage

1 Introduction and outline

The increasing application of reactive polymer systems like epoxy- or PU-adhesives in automotive, electronics or aerospace industry necessitates the development of simulation concepts and constitutive models that consider the time-dependence exhibited by relevant mechanical properties like the elastic stiffness, viscosity or relaxation time. Uncured polymer solutions usually behave as deformable viscous liquids mainly incapable of sustaining any load other than hydrostatic. During the curing process, polymer chains form from the constituents of the solution, possibly cross-link to each other and stiffness, viscosity and molecular weight increase. To especially account for temporal evolutions of inelastic material properties is not only necessary until the material has passed its gel point, but also due to the fact that almost every cured polymer possesses rate dependent creep and relaxation effects. Both are highly dependent on the particular structure and are observable as rather fast processes with relaxation times in the order of seconds, e.g. for elastomers, as well as very slow ones taking several days like in epoxies.

Concerning previous contributions on modelling and simulation of curing phenomena in polymers we refer to the literature cited in the prequels [1] and [2] of this work. Real-world applications of the simulation concept proposed here would be reliant on experimental data concerning the evolution of material parameters during the curing process, e.g. on time-dependent values for stiffness, viscosity and/or relaxation time. Unfortu-

nately, the number of publications on this field still is rather limited, some references have been given in [2].

The foundation for the viscoelastic curing models proposed here is provided by the following hypoelastic constitutive equation for the rate of the Piola-Kirchhoff stress tensor $\boldsymbol{S}$

$$\dot{\boldsymbol{S}}(t) = \frac{1}{2}\mathbb{C}(t) : \dot{\boldsymbol{C}}(t)\,, \tag{1}$$

which describes the behaviour of elastically curing materials. This equation has been phenomenologically motivated in [2] for the case of small strains, its present format and thermodynamical consistency were introduced and proven in [1]. With $\boldsymbol{C} = \boldsymbol{F}^t \cdot \boldsymbol{F}$ and $\mathbb{C} = 4\partial^2\Psi/\partial\boldsymbol{C}^2$ the right Cauchy-Green strain tensor and the *stiffness operator* resulting from an arbitrary free energy density Ψ are denoted. Some attention should be paid to the fact that $\boldsymbol{C}$ is only dependent on the time scale of the loading history, while $\mathbb{C}$ is additionally dependent on the curing progress. For the iterative solution of boundary value problems it is advisable to operate with the discrete solution of Eq. (1), i.e.

$$\boldsymbol{S}^{n+1} = \boldsymbol{S}^n + \frac{1}{2}\mathbb{C}^{n+1} : [\boldsymbol{C}^{n+1} - \boldsymbol{C}^n] \tag{2}$$

which results from implicit Euler backward integration. Furthermore, iterative schemes like the Newton-Raphson method require a consistent linearisation of (2) with respect to changes in strain, the so-called *tangent operator* relating strain and stress increments. For the present case this reads

$$\mathbb{E}^{n+1} = 2\frac{\partial \boldsymbol{S}^{n+1}}{\partial \boldsymbol{C}^{n+1}} = \mathbb{C}^{n+1} + [\boldsymbol{C}^{n+1} - \boldsymbol{C}^n] : \mathfrak{A}^{n+1}\,, \tag{3}$$

whereas the sixth-order tensor $\mathfrak{A}^{n+1} = \partial\mathbb{C}^{n+1}/\partial\boldsymbol{C}^{n+1}$ describes changes of the cure dependent stiffness operator with respect to the current strain.

By utilising the above equations, the subsequent Sections 2 and 3 extend a phenomenological (Neo-Hooke) and a micromechanical (21-chain) viscoelasticity model towards the simulation of curing materials. Both approaches share an important assumption that is frequently used in modelling finite viscoelasticity, i.e. the additive decomposition of the free energy density into (elastic) equilibrium and (viscous) non-equilibrium parts:

$$\Psi = \Psi_{eq} + \Psi_{neq}\,. \tag{4}$$

This energy decomposition leads to a corresponding decomposition of the stress response and, accordingly, of the tangent operator:

$$\boldsymbol{S} = \boldsymbol{S}_{eq} + \boldsymbol{S}_{neq} \quad , \quad \mathbb{E} = \mathbb{E}_{eq} + \mathbb{E}_{neq}\,. \tag{5}$$

The stress decomposition can in turn be motivated by classical rheological models like the Maxwell element and the three-element standard solid – that have extensively been used already for our small strain curing models [2]. The main difference between phenomenological and micromechanical viscoelasticity is twofold: While the latter utilises different formats for the two parts of the free energy density that are both dependent on the same list of arguments, which itself consists of strain-like quantities, the former usually assumes the same functional relation for Ψ_{eq} and Ψ_{neq}, but in terms of different variables that stem from kinematical considerations, mostly a multiplicative decomposition of the deformation gradient. For both cases, the viscoelastic Neo-Hooke and the 21-chain model, the respective governing equations for curing simulations as well as the details necessary for an implementation in finite element codes, i.e. the corresponding tangent operators, will be derived.

Section 4 will then discuss two different approaches to capture one of the most important effects in polymer curing, i.e. the reduction of specific volume, the so-called *curing shrinkage*. To this end, both the application of a pre-defined strain-like shrinkage function as well as a multiplicative decomposition of the deformation gradient are investigated. The final Section 5 presents some numerical examples demonstrating that the models proposed here are well suited to reproduce relevant phenomena in polymer curing.

2 Phenomenological example: viscoelastic Neo-Hooke curing model

As mentioned before, phenomenological viscoelasticity usually applies the same format to both parts of the free energy density, which is the compressible Neo-Hooke model in the present case. The different lists of arguments result from the kinematical assumption that a superposition of elastic and irreversible processes can be captured by multiplicatively decomposing the deformation gradient like

$$\boldsymbol{F} = \boldsymbol{F}_e \cdot \boldsymbol{F}_v\,, \tag{6}$$

whereas $\boldsymbol{F}_e$ describes elastic deformations and $\boldsymbol{F}_v$ can be understood as an internal variable defining the current state of a local stress-free intermediate configuration representing a relaxation mechanism like e.g. in a standard Maxwell element. Materials exhibiting multiple relaxation mechanisms can be modelled by extending Eq. (6) to multiple mechanisms of the form $\boldsymbol{F} = \boldsymbol{F}_e^i \cdot \boldsymbol{F}_v^i$, cf. e.g. Lubliner [12] or Reese & Govindjee [6]. The decomposition of $\boldsymbol{F}$ provides two strain

measures, i.e. the elastic and the viscous right Cauchy-Green tensor $\boldsymbol{C}_e$ and $\boldsymbol{C}_v$, respectively:

$$\boldsymbol{C}_e = \boldsymbol{F}_e^t \cdot \boldsymbol{F}_e = \boldsymbol{F}_v^{-t} \cdot \boldsymbol{C} \cdot \boldsymbol{F}_v^{-1} \quad , \quad \boldsymbol{C}_v = \boldsymbol{F}_v^t \cdot \boldsymbol{F}_v \,, \tag{7}$$

the latter describing the inelastic strains in the dashpot of the Maxwell element. The two parts of free energy density (4) are then usually assumed to depend on these strain measures according to

$$\Psi = \Psi_{eq}(\boldsymbol{C}) + \Psi_{neq}(\boldsymbol{C}_e = \boldsymbol{F}_v^{-t} \cdot \boldsymbol{C} \cdot \boldsymbol{F}_v^{-1}) \,. \tag{8}$$

The corresponding constitutive equations can be derived from the entropy inequality which, in case of the here assumed isothermal processes, reduces to the dissipation or Clausius-Duhem inequality

$$\boldsymbol{S} : \dot{\boldsymbol{C}} - 2\,\dot{\Psi} \geq 0 \,, \tag{9}$$

where $(\dot{\bullet})$ denotes the material time derivative. After some algebraic manipulations and by exploiting Eq. (6), this can in turn be particularised to

$$\begin{aligned} &\left[\boldsymbol{S} - 2\frac{\partial \Psi_{eq}}{\partial \boldsymbol{C}} - 2\boldsymbol{F}_v^{-1} \cdot \frac{\partial \Psi_{neq}}{\partial \boldsymbol{C}_e} \cdot \boldsymbol{F}_v^{-t}\right] : \frac{1}{2}\dot{\boldsymbol{C}} \\ &- \frac{\partial \Psi_{neq}}{\partial \boldsymbol{C}_e} : \frac{\partial \boldsymbol{C}_e}{\partial \boldsymbol{F}_v} : \dot{\boldsymbol{F}}_v \;\geq\; 0 \,, \end{aligned} \tag{10}$$

cf. e.g. [9] for a detailed derivation. From this, the standard argumentation due to Coleman and Gurtin [10] yields the conditional equations for the equilibrium and non-equilibrium stresses in Eq. $(5)_1$ as

$$\boldsymbol{S} = 2\frac{\partial \Psi_{eq}}{\partial \boldsymbol{C}} + 2\boldsymbol{F}_v^{-1} \cdot \frac{\partial \Psi_{neq}}{\partial \boldsymbol{C}_e} \cdot \boldsymbol{F}_v^{-t} =: \boldsymbol{S}_{eq} + \boldsymbol{S}_{neq} \,. \tag{11}$$

For the **first part** $\boldsymbol{S}_{eq}$ we now substitute the elastic Neo-Hookean curing model from [1], i.e. the equilibrium stress of the viscoelastic curing model is updated according to

$$\boldsymbol{S}_{eq}^{n+1} = \boldsymbol{S}_{eq}^{n} + \frac{1}{2}\mathbb{C}_{eq}^{n+1} : \left[\boldsymbol{C}^{n+1} - \boldsymbol{C}^{n}\right] \,, \tag{12}$$

whereas the current equilibrium stiffness operator $\mathbb{C}_{eq}^{n+1}$ has to be computed from the underlying compressible Neo-Hookean free energy density

$$\Psi_{eq} = \Psi_{eq}(\boldsymbol{C}, J) = \frac{\kappa}{2}\ln^2 J - \mu \ln J + \frac{\mu}{2}\left[I_1 - 3\right] \tag{13}$$

containing the *cure dependent* elastic Lamé parameters κ and μ, the first invariant $I_1 = \boldsymbol{C} : \boldsymbol{I}$ of the right Cauchy-Green tensor and $J = \det\boldsymbol{F}$. The particular forms of the required current stiffness and tangent operator have been shown in [1] to read

$$\mathbb{C}_{eq}^{n+1} = \kappa^{n+1}\mathbb{A} - 2\left[\mu^{n+1} - \kappa^{n+1}\ln J\right]\mathbb{B} \tag{14}$$

$$\mathbb{E}_{eq}^{n+1} = \mathbb{C}_{eq}^{n+1} + \left[\boldsymbol{C}^{n+1} - \boldsymbol{C}^{n}\right] : \mathfrak{A}^{n+1} \quad \text{with} \tag{15}$$

$$\mathfrak{A}^{n+1} = \kappa^{n+1}\left[\mathfrak{B} + 2\ln J\mathfrak{C} + \mathbb{B} \otimes \boldsymbol{C}^{-1}\right] - 2\mu^{n+1}\mathfrak{C} \,, \tag{16}$$

cf. Eqns. (16, 17) and (20, 21) in [1] for the componentwise representations of the auxiliary quantities

$$\mathbb{A} = \boldsymbol{C}^{-1} \otimes \boldsymbol{C}^{-1} \quad , \quad \mathfrak{B} = \partial\mathbb{A}/\partial\boldsymbol{C} \tag{17}$$

$$\mathbb{B} = \partial\boldsymbol{C}^{-1}/\partial\boldsymbol{C} \quad , \quad \mathfrak{C} = \partial\mathbb{B}/\partial\boldsymbol{C} \,. \tag{18}$$

For the **second part** $\boldsymbol{S}_{neq}$ of constitutive equation (11), i.e. the inelastic stress response, we resort again to the compressible Neo-Hookean ansatz (13), which is now, according to Eq. (8), dependent on the elastic right Cauchy-Green strain tensor:

$$\begin{aligned} \Psi_{neq} &= \Psi_{neq}(\boldsymbol{C}_e = \boldsymbol{F}_v^{-t} \cdot \boldsymbol{C} \cdot \boldsymbol{F}_v^{-1}, J_e) \\ &= \frac{\kappa_e}{2}\ln^2 J_e - \mu_e \ln J_e + \frac{\mu_e}{2}\left[I_{1e} - 3\right] \,. \end{aligned} \tag{19}$$

Therein, $I_{1e} = \boldsymbol{C}_e : \boldsymbol{I}$ and $J_e = \sqrt{\det\boldsymbol{C}_e}$ and the two additional Lamé parameters κ_e and μ_e are assumed to be *cure independent*, i.e. constant. The desired non-equilibrium stress follows again by evaluation of (11) from which one obtains

$$\begin{aligned} \boldsymbol{S}_{neq} &= 2\boldsymbol{F}_v^{-1} \cdot \frac{\partial \Psi_{neq}}{\partial \boldsymbol{C}_e} \cdot \boldsymbol{F}_v^{-t} \\ &= \boldsymbol{F}_v^{-1} \cdot \left[\kappa_e \ln J_e \boldsymbol{C}_e^{-1} + \mu_e\left[\boldsymbol{I} - \boldsymbol{C}_e^{-1}\right]\right] \cdot \boldsymbol{F}_v^{-t} \\ &= \kappa_e \ln J_e\, \boldsymbol{C}^{-1} + \mu_e\left[\boldsymbol{C}_v^{-1} - \boldsymbol{C}^{-1}\right] \end{aligned} \tag{20}$$

after recalling that $\partial I_{1e}/\partial\boldsymbol{C}_e = \boldsymbol{I}$ and $\partial J_e/\partial\boldsymbol{C}_e = \frac{1}{2}J_e\boldsymbol{C}_e^{-1}$ and exploiting Eq. (7). Note that the cure dependence of the inelastic material properties has not been considered yet but is implicitly present in the strain-like internal variable $\boldsymbol{C}_v$, whose current value needs to be determined now. To this end, exploiting the second part

$$-\frac{\partial \Psi_{neq}}{\partial \boldsymbol{C}_e} : \frac{\partial \boldsymbol{C}_e}{\partial \boldsymbol{F}_v} : \dot{\boldsymbol{F}}_v \geq 0 \tag{21}$$

of dissipation inequality (10) provides, after some rigorous mathematical manipulations the details of which can be found e.g. in [6], a non-linear evolution equation for $\boldsymbol{C}_v$. This equation can in turn be linearised according to [7] which yields a rather simple ordinary differential equation that is frequently used in finite linear viscoelasticity [9,11,13,14]:

$$\dot{\boldsymbol{C}}_v = T^{-1}\left[\boldsymbol{C} - \boldsymbol{C}_v\right] . \tag{22}$$

It describes the evolution of the internal variable $\boldsymbol{C}_v$ in terms of $\boldsymbol{C}$ and an additional material parameter, the relaxation time T which becomes time-dependent, i.e. $T = T(t)$ in case of curing materials:

$$\dot{\boldsymbol{C}}_v = T(t)^{-1}\left[\boldsymbol{C} - \boldsymbol{C}_v\right] . \tag{23}$$

Application of the implicit Euler-backward integration scheme then provides the following discrete update equation for $\boldsymbol{C}_v$:

$$\boldsymbol{C}_v^{n+1} = \underbrace{\frac{\Delta t}{T^{n+1} + \Delta t}}_{=:\,\omega^{n+1}} \boldsymbol{C}^{n+1} + \frac{T^{n+1}}{T^{n+1} + \Delta t}\boldsymbol{C}_v^{n} \,, \tag{24}$$

whereas T^{n+1} denotes the current relaxation time and $\Delta t = t_{n+1} - t_n$ is the current time step length. Inserting this into (20) concludes, together with (12) and (14), the constitutive relations for the viscoelastic Neo-Hookean curing model.

To obtain the remaining non-equilibrium part $\mathbb{E}_{neq}$ of tangent operator $(5)_2$, the derivative of the non-equilibrium stress $(20)_3$ with respect to the strain has to be computed. From the chain rule and some tensor calculus we find

$$\begin{aligned}\mathbb{E}_{neq} &= 2\frac{\partial \boldsymbol{S}_{neq}}{\partial \boldsymbol{C}} \\ &= 2\kappa_e \ln J_e \frac{\partial \boldsymbol{C}^{-1}}{\partial \boldsymbol{C}} + 2\kappa_e \boldsymbol{C}^{-1} \otimes \frac{\partial \ln J_e}{\partial \boldsymbol{C}} \\ &\quad + 2\mu_e \left[\frac{\partial \boldsymbol{C}_v^{-1}}{\partial \boldsymbol{C}_v} : \frac{\partial \boldsymbol{C}_v}{\partial \boldsymbol{C}} - \frac{\partial \boldsymbol{C}^{-1}}{\partial \boldsymbol{C}} \right] . \end{aligned} \tag{25}$$

Therein, abbreviation $\mathbb{B}$ as given in Eq. $(18)_1$ may be used and $\partial \boldsymbol{C}_v / \partial \boldsymbol{C} = \omega \mathbb{I}^{sym}$ holds with $\mathbb{I}^{sym} = \frac{1}{2}[\delta_{ik}\delta_{jl} + \delta_{il}\delta_{jk}]$ since only the first term in Eq. (24) is dependent on the current strain. Furthermore, we define $\mathbb{D} := \partial \boldsymbol{C}_v^{-1} / \partial \boldsymbol{C}_v$, the component-wise representation of which is given by

$$(\mathbb{D})_{ijkl} = -\frac{1}{2} \left[(\boldsymbol{C}_v^{-1})_{ik} (\boldsymbol{C}_v^{-1})_{jl} + (\boldsymbol{C}_v^{-1})_{il} (\boldsymbol{C}_v^{-1})_{jk} \right] . \tag{26}$$

The multiplicative decomposition of the deformation gradient implies $J = J_e J_v$, i.e. $\ln J_e = \ln J - \ln J_v$. Using this, the derivative $\partial \ln J_e / \partial \boldsymbol{C}$ in (25) can, due to the chain rule and $\partial J_{(v)} / \partial \boldsymbol{C}_{(v)} = \frac{1}{2} \boldsymbol{C}_{(v)}^{-1}$, be simplified to

$$\frac{\partial \ln J_e}{\partial \boldsymbol{C}} = \frac{1}{J} \frac{\partial J}{\partial \boldsymbol{C}} - \frac{1}{J_v} \frac{\partial J_v}{\partial \boldsymbol{C}} = \frac{1}{2} \boldsymbol{C}^{-1} - \frac{\omega}{2} \boldsymbol{C}_v^{-1} . \tag{27}$$

Insertion of (27) into (25) finally yields the current non-equilibrium tangent operator

$$\begin{aligned}\mathbb{E}_{neq}^{n+1} &= \kappa_e \left[2 \ln J_e \, \mathbb{B} + \boldsymbol{C}^{-1} \otimes \left[\boldsymbol{C}^{-1} - \omega^{n+1} \boldsymbol{C}_v^{-1} \right] \right] \\ &\quad + 2\mu_e \left[\omega^{n+1} \mathbb{D} - \mathbb{B} \right] , \end{aligned} \tag{28}$$

which concludes, together with Eqns. (18), (24), (26) and (15), the derivation of the viscoelastic Neo-Hooke curing model. Note that double contractions with $\mathbb{I}^{sym}$ can be omitted since all strain measures are symmetric by definition.

3 Micromechanical example: viscoelastic 21-chain curing model

Similar to our previous contribution [1] on elastic curing models, we will in the following resort to the 21-chain micro-macro unit sphere model developed by Miehe and co-workers, now in its viscoelastic version published in [3]. Thereby, all parts of the model that describe chain interactions, which is done by considering the contraction of the cross section of a tube confining the polymer chain, are neglected for the sake of simplicity. Furthermore, we assume affine relationsships between micro-kinematical quantities and their continuum counterparts for both the elastic and viscolastic networks, not only for the latter. The extension necessary to capture viscous curing behaviour is, once more, based on the time dependence of the viscous material parameters, i.e. the relaxation time.

The 21-chain viscoelastic curing model utilises the same assumptions on the decomposition of free energy density, stress response and tangent operator that are reflected by Eqns. (4) and (5). For the **equilibrium part**, the compressible energy density Ψ_{eq} as given by Eq. (26) in [1] is used, i.e.

$$\Psi_{eq} = \sum_{i=1}^{21} \mu N w_i \left[\gamma_i \lambda_i^r + \ln \frac{\gamma_i}{\sinh \gamma_i} \right] + \frac{\kappa}{2} \ln^2 J - \mu \ln J , \tag{29}$$

which represents a homogenisation of the behaviour of 21 Langevin chains oriented uniformly within a unit sphere and each consisting of a cure dependent number $N = N(t)$ of Kuhn segments [15]. While the two latter parts describe the volumetric behaviour in terms of the usual, time dependent Lamé parameters, the sum is combining the chain contributions in terms of their orientation dependent relative stretches $\lambda_i^r = \sqrt{N^{-1} \boldsymbol{C} : [\boldsymbol{t}_i \otimes \boldsymbol{t}_i]}$ and a Padé approximation of the inverse Langevin function: $\gamma_i := \mathcal{L}^{-1}(\lambda_i^r) \approx \lambda_i^r [3 - (\lambda_i^r)^2][1 - (\lambda_i^r)^2]^{-1}$. The weights w_i and direction vectors $\boldsymbol{t}_i$ are given in the appendix of [1]. The corresponding current equilibrium stress $\boldsymbol{S}_{eq}^{n+1}$ is computed according to Eq. (12) whereas the current stiffness operator

$$\begin{aligned}\mathbb{C}_{eq}^{n+1} &= \sum_{i=1}^{21} w_i \frac{4\mu^{n+1} N^{n+1}}{\left[N^{n+1} - \lambda_i^2 \right]^2} \left[\boldsymbol{t}_i \otimes \boldsymbol{t}_i \otimes \boldsymbol{t}_i \otimes \boldsymbol{t}_i \right] \\ &\quad + \kappa^{n+1} \mathbb{A} - 2 \left[\mu^{n+1} - \kappa^{n+1} \ln J \right] \mathbb{B} \end{aligned} \tag{30}$$

has to be inserted, cf. also Eq. (27) in [1]. The current equilibrium tangent operator $\mathbb{E}_{eq}^{n+1}$ again follows relation (15) and additionally requires

$$\begin{aligned}\mathfrak{A}^{n+1} &= \sum_{i=1}^{21} w_i \frac{8\mu^{n+1} N^{n+1}}{\left[N^{n+1} - \lambda_i^2 \right]^3} \left[\boldsymbol{t}_i \otimes \boldsymbol{t}_i \otimes \boldsymbol{t}_i \otimes \boldsymbol{t}_i \otimes \boldsymbol{t}_i \otimes \boldsymbol{t}_i \right] \\ &\quad + \kappa^{n+1} \left[\mathfrak{B} + 2 \ln J \mathfrak{C} + \mathbb{B} \otimes \boldsymbol{C}^{-1} \right] - 2\mu^{n+1} \mathfrak{C} \end{aligned} \tag{31}$$

with the chain stretch $\lambda_i = \sqrt{N} \lambda_i^r$ and abbreviations $\mathbb{A}, \mathbb{B}, \mathfrak{B}, \mathfrak{C}$ as used in the previous section. Concerning the temporal evolution of the relevant material parameters and especially their interdependences the interested reader is referred to Section 5 in [1].

The **non-equilibrium part** realises inelastic behaviour by superimposing a network of viscoelastic

chains that are connected via entanglements to the elastic network, which itself has been the basis for Eq. (29). These chains are not only deformed with the elastic network but additionally able to relax their stretch state by untangling their loose ends, which in turn increases the number of active Kuhn segments, cf. [16,3] for a schematic visualisation. This dynamic process can be modelled phenomenologically by extending the elastic free energy density φ_i of a single chain oriented along $\boldsymbol{t}_i$ (compare Eq. (24) in [1]) with

$$\varphi_i^v = \frac{\mu_v}{2}\left[\ln\lambda_i - \varepsilon_i\right]^2 \quad , \quad i = 1, ..., 21\,, \tag{32}$$

as proposed by Miehe and co-workers [3]. The tube constraint part has again been neglected and μ_v, ε_i denote a cure independent, phenomenological material parameter and a strain-like internal variable governing the non-equilibrium stress of the chain, respectively. Relation (32) can easily be extended towards multiple relaxation mechanisms if reformulated as a sum, similar to the addition of further Maxwell elements in the phenomenological case. We omit this possibility for simplicity and restrict all following considerations to only one relaxation mechanism.

The corresponding continuum non-equilibrium free energy Ψ_{neq} is now obtained from the same procedure of homogenising chain contributions over the unit sphere that already led to (29), i.e.

$$\Psi_{neq} = \langle\varphi_i^v\rangle = \frac{1}{2}\sum_{i=1}^{21} w_i\mu_v\left[\ln\lambda_i - \varepsilon_i\right]^2 \tag{33}$$

where the ε_i successively relax the initial elastic chain stretches $\lambda_i = \sqrt{\boldsymbol{C} : [\boldsymbol{t}_i \otimes \boldsymbol{t}_i]}$. Energetically conjugated micro forces driving the evolution of the strain-like ε_i can, according to Miehe et al. [3], be defined by

$$\beta_i := -\frac{\partial\varphi_i^v}{\partial\varepsilon_i} = \mu_v\left[\ln\lambda_i - \varepsilon_i\right]\,. \tag{34}$$

By assuming appropriate functions to describe the dissipation at the chain level and after some calculations the details of which can be found in [3] or [5], the constraint of non-negative micro dissipation provides the following non-linear evolution equation for β_i:

$$\dot{\beta}_i + \frac{\beta_i}{T}\left|\beta_i\right|^{\delta-1} - \frac{\mu_v}{\lambda_i}\dot{\lambda}_i = 0 \quad \text{with} \quad \beta_i(t=0) = 0\,. \tag{35}$$

Therein, $\delta > 0$ denotes a constant material parameter while $|\bullet|$ is the absolute value relieved of units. To describe curing materials, the relaxation time T in (35) is again set to be cure dependent, i.e. $T = T(t)$, and assumed to evolve according to an exponential saturation function as proposed for our small-strain curing model, cf. Eq. (38) in [2]:

$$T(t) = T_0 + \left[T_\infty - T_0\right]\left[1 - \exp(-\kappa_\tau t)\right]\,. \tag{36}$$

Here, T_0, T_∞ are initial and final relaxation time, respectively, and κ_τ describes the reduction rate of the viscosity during curing, i.e. the decrease of the untangling velocity of the chains. Evolution equation (35) has to be solved iteratively at every Gauss point for every time step and chain orientation $\boldsymbol{t}_i$, e.g. by Newton's method, for which a detailed recipe is given in Table 1. Regarding memory requirements it is worth noting that all chain forces β_i and stretches λ_i from the previous load step have to be stored. The current non-equilibrium stress tensor then reads

$$\boldsymbol{S}_{neq}^{n+1} = 2\frac{\partial\Psi_{neq}}{\partial\boldsymbol{C}} = \sum_{i=1}^{21} w_i\frac{\beta_i^{n+1}}{\lambda_i}\left[\boldsymbol{t}_i \otimes \boldsymbol{t}_i\right] \tag{37}$$

and the current non-equilibrium tangent operator follows accordingly as twice the derivative of the stress with respect to the strain, i.e.

$$\mathbb{E}_{neq}^{n+1} = \sum_{i=1}^{21} w_i\left[\frac{c_i^{n+1}}{\lambda_i^2} - \frac{\beta_i^{n+1}}{\lambda_i^3}\right]\left[\boldsymbol{t}_i \otimes \boldsymbol{t}_i \otimes \boldsymbol{t}_i \otimes \boldsymbol{t}_i\right]\,, \tag{38}$$

cf. again to [3], [5] for detailed derivations. For the sake of clarity, only terms containing cure dependent quantities are indicated by superscript $n{+}1$ in both equations.

4 Modelling curing shrinkage

One of the prominent phenomena in polymer curing is the *shrinkage effect*, i.e. the reduction of the specific volume due to chain growth and/or cross linking. In case of specimen held within fixed boundaries during curing, this can lead to significant residual stresses and/or strains, where the former may even surpass the plastic yield strength. The relevance of this effect is dependent on the time of gelation, before which the material can hardly develop any stresses, as well as on the inelastic characteristics afterwards which may allow relaxation of the shrinkage stresses. Especially in case of epoxies with high relaxation times but essentially elastoplastic behaviour, the influences of the curing shrinkage may even impede certain applications like structural bonding in automotive frame and body construction due to unacceptable sheet deformation.

Two approaches to incorporate the shrinkage effect into constitutive models have been proposed in the literature so far: **(1)** the superposition of an exponentially decaying shrinkage strain function, which has been introduced by Kiasat [17], and **(2)** a multiplicative decomposition of the deformation gradient, advocated by

(i) Given from previous time step t_n are stretch and strain for all chain orientations $\boldsymbol{t}_i$, i.e. $\left\{\left(\lambda_i^n, \beta_i^n\right) \mid i = 1, ..., 21\right\}$.

(ii) Compute current chain stretches $\lambda_i^{n+1} = \sqrt{\boldsymbol{C}^{n+1} : [\boldsymbol{t}_i \otimes \boldsymbol{t}_i]}$ with current deformation gradient: $\boldsymbol{C}^{n+1} = \boldsymbol{F}^t(t_{n+1}) \cdot \boldsymbol{F}(t_{n+1})$.

(iii) Determine β_i^{n+1} by applying Newton's method to the Euler backward solution of Eq. (35), i.e. the non-linear equation

$$\beta_i^{n+1}\left[1 + \frac{\Delta t}{T^{n+1}}\left|\beta_i^{n+1}\right|^{\delta-1}\right] - \beta_i^n + \mu_v\left[\frac{\lambda_i^n}{\lambda_i^{n+1}} - 1\right] =: r_i(\beta_i^{n+1}) \stackrel{!}{=} 0 \quad \text{is solved by iteratively updating } \beta_i^{n+1} \text{ according to}$$

$${}^k\beta_i^{n+1} = {}^{k-1}\beta_i^{n+1} - \frac{r_i({}^{k-1}\beta_i^{n+1})}{r_i'({}^{k-1}\beta_i^{n+1})} \quad , \quad k = 1, ... \quad , \quad {}^0\beta_i^{n+1} := \beta_i^n \quad , \quad \text{until} \quad r_i({}^k\beta_i^{n+1}) < tol \quad \text{and where}$$

$$r_i'({}^k\beta_i^{n+1}) = \left[1 + \frac{\Delta t}{T^{n+1}}\left|{}^k\beta_i^{n+1}\right|^{\delta-1}\right] + \frac{\Delta t}{T^{n+1}}[\delta - 1]\left|{}^k\beta_i^{n+1}\right|^{\delta-3}\left[\beta_i^{n+1}\right]^2.$$

(iv) Compute the current chain tangent moduli $c_i := d\beta_i/d\lambda_i$ from $c_i^{n+1} = \dfrac{\mu_v}{\left[\lambda_i^{n+1}\right]^2 r_i'(\beta_i^{n+1})} - \dfrac{\beta_i^{n+1}}{\lambda_i^{n+1}}$.

(v) Insert the current β_i^{n+1}, c_i^{n+1} into the stress tensor and tangent operator, i.e. equations (37) and (38), respectively.

Table 1 Update procedure for the non-equilibrium micro forces β_i

Lion and Höfer [18]. In the following subsections, both ansatzes will be incorporated to the above proposed methods for curing simulations.

4.1 Shrinkage strain function

This rather basic, nonetheless successful approach to consider volume shrinkage utilises a prescribed, cure/time dependent volumetric strain function which is simply superimposed to the current deformation state during the simulation. Kiasat [17], for example, proposed the following, exponentially decaying scalar function

$$C_s(t) = p_1 \exp\left(-\left[\frac{p_2}{t}\right]^{p_3}\right) + p_4 \exp\left(-\left[\frac{p_5}{t}\right]^{p_6}\right), \quad (39)$$

which is governed by six parameters p_i that have to be determined experimentally. A specification of this function, which is also used in the forthcoming examples, is plotted in Fig. 1.

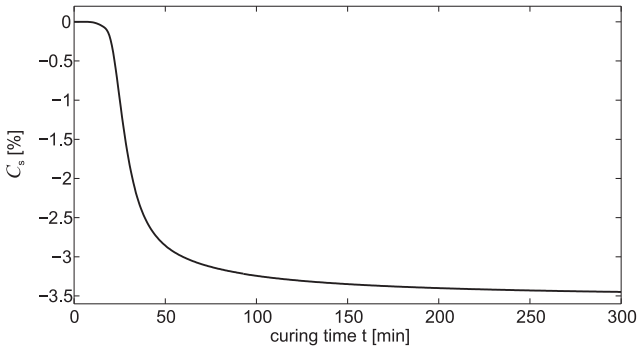

Fig. 1 Evolution of shrinkage function (39) in case of $[p_1, p_2, p_3, p_4, p_5, p_6]$ = [-1.129, 37.36 min, 1.261, -2.402, -25.74 min, 4.611]

The incorporation of this in the form of a volumetric strain to the above proposed curing models is realised by modifying update equation (12) for the current equilibrium stress according to

$$\boldsymbol{S}_{eq}^{n+1} = \boldsymbol{S}_{eq}^n + \frac{1}{2}\mathbb{C}_{eq}^{n+1} : [[\boldsymbol{C}^{n+1} - C_s^{n+1}\boldsymbol{I}] - [\boldsymbol{C}^n - C_s^n\boldsymbol{I}]], \quad (40)$$

i.e. a correction of both the previous and current strain state is introduced. Since C_s is independent of $\boldsymbol{C}$, the linearisation of (40) with respect to the right Cauchy-Green strain provides the correspondingly modified current equilibrium tangent operator:

$$\mathbb{E}_{eq}^{n+1} = \mathbb{C}_{eq}^{n+1} + [[\boldsymbol{C}^{n+1} - C_s^{n+1}\boldsymbol{I}] - [\boldsymbol{C}^n - C_s^n\boldsymbol{I}]] : \mathfrak{A}^{n+1}. \quad (41)$$

To clarify the procedure, the incorporation of volume shrinkage has been restrained to the equilibrium material response. A consideration of shrinkage within the non-equlilibrium part is straight-forward and will be illustrated by an example in Section 5 to demonstrate the relaxation of shrinkage stresses in viscoelastic materials.

4.2 Multiplicative decomposition

The application of a multiplicative decomposition of the deformation gradient within the context of curing and shrinkage has first been advocated by Lion and Höfer [18]. We will here omit the originally included thermal part and restrict ourselves to decomposing the deformation gradient into two parts, i.e. a stress producing mechanical part and a volume reducing shrinkage part:

$$\boldsymbol{F} = \boldsymbol{F}_m \cdot \boldsymbol{F}_s \quad \text{with} \quad \boldsymbol{F}_s := [1 + \alpha s]^{1/3}\boldsymbol{I}\,. \quad (42)$$

Therein, $\alpha \in [0,1]$ denotes the degree of cure, cf. [2], and $s \leq 0$ is a time dependent parameter controlling the magnitude of the shrinkage. Note that this ansatz can be (and is frequently) used to model e.g. growth phenomena in biomechanics [19]. Similar to phenomenological viscoelasticity, the following decomposition of the right Cauchy-Green tensor is implied by (42):

$$\boldsymbol{C} = \boldsymbol{F}^t \cdot \boldsymbol{F} = \boldsymbol{F}_s^t \cdot \boldsymbol{F}_m^t \cdot \boldsymbol{F}_m \cdot \boldsymbol{F}_s =: \boldsymbol{F}_s^t \cdot \boldsymbol{C}_m \cdot \boldsymbol{F}_s \qquad (43)$$

which provides the conditional equation for the mechanical right Cauchy-Green strain as

$$\boldsymbol{C}_m = \boldsymbol{F}_m^t \cdot \boldsymbol{F}_m = \boldsymbol{F}_s^{-t} \cdot \boldsymbol{C} \cdot \boldsymbol{F}_s^{-1} = [1+\alpha s]^{-2/3} \boldsymbol{C}. \quad (44)$$

From the ususal thermodynamical argumentation that has already been used in the case of phenomenological viscoelasticity, the corresponding Piola-Kirchhoff stress is obtained to read

$$\boldsymbol{S} = \boldsymbol{F}_s^{-1} \cdot 2 \frac{\partial \Psi_m}{\partial \boldsymbol{C}_m} \cdot \boldsymbol{F}_s^{-t} = [1+\alpha s]^{-2/3} \boldsymbol{S}_m, \qquad (45)$$

with the cure dependent mechanical free energy density Ψ_m. Thus, the total stress resulting from mechanical load and superimposed curing shrinkage is equal to the purely mechanical stress $\boldsymbol{S}_m$, as computed e.g. from Eq. (11) with (12) and (20), pre-multiplied by $\boldsymbol{F}_s^{-2}$. More generally, this can be understood as a pull-back operation from the stress-free intermediate configuration to the reference configuration.

The necessary tangent operator is again obtained from linearising the stress with respect to the strain for which the chain rule yields

$$\begin{aligned} \mathbb{E} &= 2 \frac{\partial \boldsymbol{S}}{\partial \boldsymbol{C}} = 2 \frac{\partial \boldsymbol{S}}{\partial \boldsymbol{C}_m} : \frac{\partial \boldsymbol{C}_m}{\partial \boldsymbol{C}} \\ &= 2 \frac{\partial \left([1+\alpha s]^{-2/3} \boldsymbol{S}_m \right)}{\partial \boldsymbol{C}_m} : \frac{\partial \left(\boldsymbol{F}_s^{-t} \cdot \boldsymbol{C} \cdot \boldsymbol{F}_s^{-1} \right)}{\partial \boldsymbol{C}} \\ &= [1+\alpha s]^{-4/3} \mathbb{E}_m, \end{aligned} \qquad (46)$$

with $\mathbb{E}_m = 2 \partial \boldsymbol{S}_m / \partial \boldsymbol{C}_m$ denoting the mechanical tangent operator that has to be calculated e.g. from Eq. (15) and (28).

5 Numerical examples

Several numerical examples are presented in this section to demonstrate that the proposed models are suitable to reproduce the mechanical behaviour of viscoelastic polymers during isothermal curing, which is, in particular, characterised by a stiffness gain, decelerating relaxation effects and a volumetric shrinkage. All simulations have been performed using a research-based in-house finite element code that has been extended by the constitutive relations and tangent operators summarised in the previous sections. First, some one-dimensional examples reflect the behaviour of a single eight-noded brick element under prescribed uniaxial stretch histories and parameter evolutions. Next, several three-dimensional simulations are presented to demonstrate both inhomogeneous deformation behaviour and the effects induced by the curing shrinkage.

Due to the lack of sufficient experimental data on the temporal evolution of material parameters we resort to arbitrary but reasonable choices. Concerning the equilibrium shear modulus μ the previously used [1] exponential saturation function, whose format is also assumed for the relaxation time, cf. Eq. (36), is applied

$$\mu(t) = \mu_0 + [\mu_\infty - \mu_0] \left[1 - \exp(-\kappa_\mu t) \right] , \qquad (47)$$

being governed by initial and final shear moduli μ_0 and μ_∞, respectively, as well as the curvature parameter κ_μ. A specification of (47) is plotted in Fig. 2. For the sake of simplicity, the elastic bulk modulus is calculated via $\kappa(t) = \frac{2}{3}\mu(t)[1+\nu][1-\nu]^{-1}$ from the prescribed shear modulus evolution, whereas a constant Poisson's ratio of $\nu = 0.35$ has been assumed. For the 21-chain model, an initial number N_0 of chain segments is prescribed and the resulting temporal evolution $N(t)$ follows from that of the shear modulus, cf. the discussion on conservation of mass in [1]. The non-equilibrium parameters κ_e, μ_e, μ_v are kept at constant values, only the relaxation time evolves according to (36).

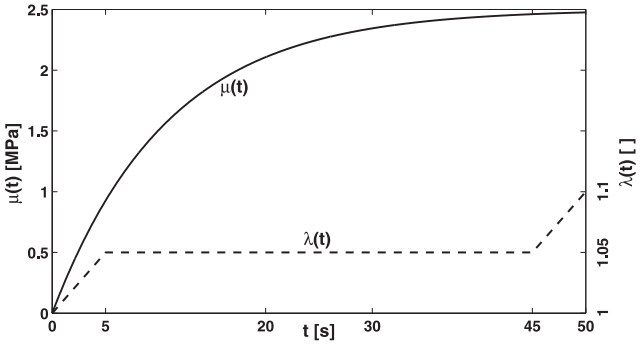

Fig. 2 Three phase load history $\lambda(t)$ and exemplary evolution of the shear modulus $\mu(t)$ with $[\mu_0, \mu_\infty, \kappa_\mu]$ =[0.0001 MPa, 2.5 MPa, 0.0925 s^{-1}]

5.1 Homogeneous one-dimensional examples

First, simple uniaxial tension tests are simulated using a single finite element to check whether the proposed curing models will correctly reproduce the gain in stiffness, the behaviour in case of the strain rate being zero and the deceleration of relaxation processes during the advancement of curing. Concerning the first two properties we consider a three phase deformation history that consists of (1) a linear increase to a (macroscopic)

stretch $\lambda = 1.05$ within the first five seconds, followed by (2) a fourty seconds holding phase and (3) another linear increase to $\lambda = 1.1$ during the last five seconds, cf. Figure (2). This load history is applied to both the compressible Neo-Hooke and 21-chain viscoelastic curing model, whereas only the elastic parameters are evolving but the relaxation time is kept fixed for the moment. Figure 3 depicts the resulting stress responses vs. time and stretch, the parameters used are given in the caption. Both models obviously behave viscoelastic, as is indicated by the decrease in stress during the holding phase. The ongoing increase in stiffness has no impact on the stress in case of a constant deformation state, which is reflected by the horizontal lines in the left-hand figures after the relaxation has reached its equilibrium. Within the right-hand side figures, the stiffness gain is clearly observable by comparing the slopes of the curves before and after the holding phase at $\lambda = 1.05$. The different magnitudes of the stress increase during the two loading phases (left-hand side figures) do also reflect this.

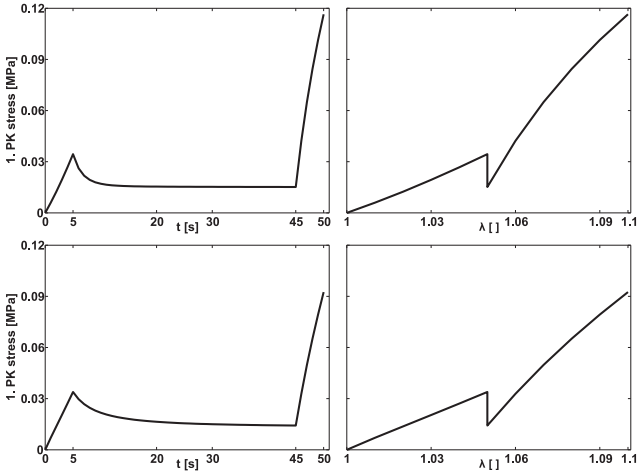

Fig. 3 Response of a curing viscoelastic material with constant relaxation time under the stretch history of Fig. 2. Piola stress vs. time **(left)** and stretch **(right)**, each for the Neo-Hooke model **(top)** with $[\mu_0, \mu_\infty, \kappa_\mu, \kappa_e, \mu_e, T, \Delta t]$ =[0.001 MPa, 0.5 MPa, 0.0925 s^{-1}, 10.5 MPa, 0.75 MPa, 3 s, 1 s] and the 21-chain model **(bottom)** with $[\mu_0, \mu_\infty, \kappa_\mu, N_0, \mu_v, T, \delta, \Delta t]$=[0.001 MPa, 0.5 MPa, 0.0925 s^{-1}, $5{\cdot}10^4$, 5.5 MPa, 1.2 s, 1.5, 1 s]

To demonstrate the effects that arise if also the viscoelastic properties are evolving, the above stretch history is modified to three linear loading phases of two seconds duration which are interleaved with two holding phases each lasting for twenty seconds. The responses are plotted in Fig. 4 and clearly indicate the desired deceleration of viscous relaxation processes for both models since the equilibrium stresses are reached much later within the second holding phases. Furthermore, slower relaxation time evolutions are also correctly captured as can be observed from the higher stress peaks at the end of each loading phase.

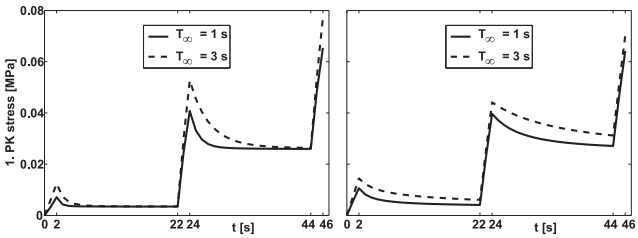

Fig. 4 Curing viscoelastic material subjected to a five phase stretch history. Piola stress vs. time for two different final relaxation times T_∞. **Left:** Neo-Hooke with $[\mu_0, \mu_\infty, \kappa_\mu, \kappa_e, \mu_e, T_0, T_\infty, \kappa_\tau, \Delta t]$ = [0.001 MPa, 0.5 MPa, 0.0925 s^{-1}, 10.5 MPa, 0.75 MPa, 0.015 s, **1 vs. 3 s**, 0.0925 s^{-1}, 1 s]. **Right:** 21-chain with $[\mu_0, \mu_\infty, \kappa_\mu, N_0, \mu_v, T_0, T_\infty, \kappa_\tau, \delta, \Delta t]$ = [0.001 MPa, 0.5 MPa, 0.0925 s^{-1}, $5{\cdot}10^4$, 5.5 MPa, 0.015 s, **1 vs. 3 s**, 0.0925 s^{-1}, 1.5, 1 s]

5.2 Inhomogeneous three-dimensional example

Concerning viscoelastic curing behaviour in three dimensions we consider a plate with a hole in its center to realise inhomogeneous stress distributions under load. Its dimensions are $60 \times 12 \times 2\,mm^3$ and the hole has a diameter of $6\,mm$. The plate is discretised by 544 eight-noded hexagonal elements and supported as depicted in Fig. 5 (most left). A uniaxial extension in x-direction is applied within 22 seconds, which is followed by 168 s of relaxation. These two steps are repeated a second time to check the evolution of elastic and viscous material properties. Figure 5 (left) depicts both the deformation and the resulting Cauchy stresses in x-direction, the latter obviously are decreasing during the holding phases. The right-hand side compares the behaviour of two nodes which are chosen such that their stress levels after the first and second loading phase are equal. The curves clearly indicate the desired deceleration of relaxation processes (curves between the dashed lines) as well as the gain in stiffness (different magnitudes of stress growth during the loading phases) and the constant stress in cases where the strain rate becomes zero (after the relaxation has reached equilibrium).

5.3 Curing shrinkage simulations

5.3.1 Shrinkage strain function

For shrinkage induced stress build-up during cure, a three-dimensional block of $20 \times 7 \times 3\,mm^3$, discretised by one hundred eight-noded brick elements, is considered. Its front and back side are kept fixed while all longitudinal sides are free to deform. The curing shrinkage

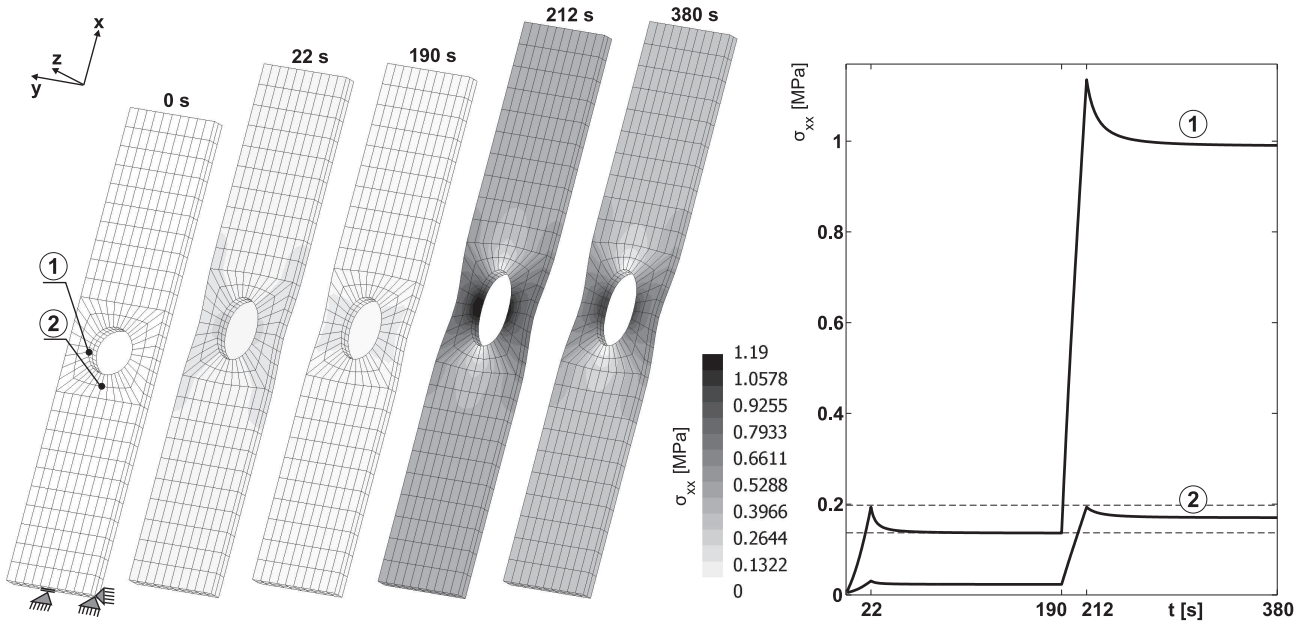

Fig. 5 Three-dimensional boundary value problem: plate with centered hole, subjected to a four phase stretch history (pull, hold, pull, hold) and modelled by the viscoelastic 21-chain curing model with $[\mu_0, \mu_\infty, \kappa_\mu, N_0, \mu_v, T_0, T_\infty, \kappa_\tau, \delta, \Delta t]$=[0.0001 MPa, 2.0 MPa, 0.0115 s^{-1}, $2{\cdot}10^6$, 10.5 MPa, 0.015 s, 4.2 s, 0.0115 s^{-1}, 1.5, 1s]. **Left:** Cauchy stress and deformation at relevant time steps. **Right:** Comparison of stress vs. time for two nodes having the same stress level at the beginning of the first and second relaxation phase, respectively. The deceleration of relaxation processes is clearly visible from the fact that node ② relaxes much slower to a higher equilibrium stress after $t = 212s$ than node ① does between $t = 22...190s$. The gain in stiffness is again reflected by the much higher stress increase during the second loading phase.

is modelled by the shrinkage strain function approach described in Sec. 4.1, which is here applied to the elastic Neo-Hooke curing model. Figure 6 depicts deformation and Cauchy-stresses after 270 minutes of curing under the assumption of Kiasat's [17] volume shrinkage function as given in Fig. 1. Both the resulting deformations and stresses do obviously attain magnitudes that should be considered carefully in design and dimensioning of structures.

5.3.2 Multiplicative decomposition

To illustrate shrinkage simulations relying on the multiplicative decomposition of the deformation gradient we adapt a setup for a thin three-dimensional plate that has been used by Retka and Höfer [20]. The plate has an extension of $40 \times 10 \times 0.5\, mm^3$ and is discretised by 800 linear brick elements. Three different bearing conditions are assumed, cf. Fig. 7, as well as a final volume reduction of ten percent, i.e. $s = -0.1$ in Eq. $(42)_2$. The degree of cure α is simply assumed to evolve according to an exponential saturation function like (47), which has already been used for shear modulus and relaxation time, whereas now $[\alpha_0, \alpha_\infty, \kappa_\alpha] = [0.0001, 1.0, 0.25\ s^{-1}]$. More sophisticated approaches for the evolution of α, as mentioned e.g. in [2], are not considered here for the sake of simplicity but are, nonetheless, straightforwardly to incorporate. Note that the initial degree of cure – as well as the initial shear modulus – has to have a small positive value for numerical reasons. Figure 7 depicts the bearing specific deformations as well as the Cauchy stresses in x-direction after twenty seconds of curing, simulated with the elastic 21-chain curing model together with the shrinkage model equations of Sec. 4.2.

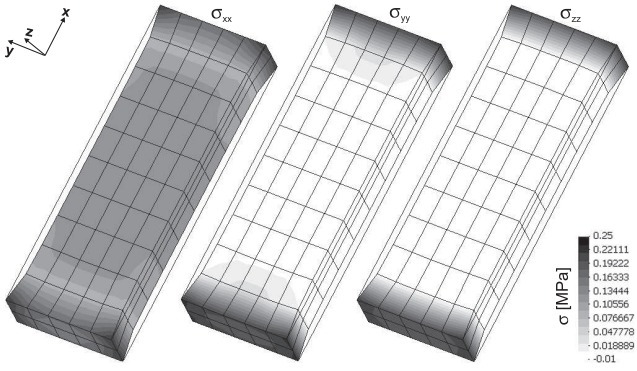

Fig. 6 Block without external load but fixed transverse ends. Deformation (scaled by two) and Cauchy stresses due to shrinkage after 270 minutes of curing. Elastic Neo-Hooke curing model with $[\mu_0, \mu_\infty, \kappa_\mu]$ =[0.0001 MPa, 1.5 MPa, 0.02 s^{-1}], extended by the shrinkage strain function approach of Sec. 4.1

.

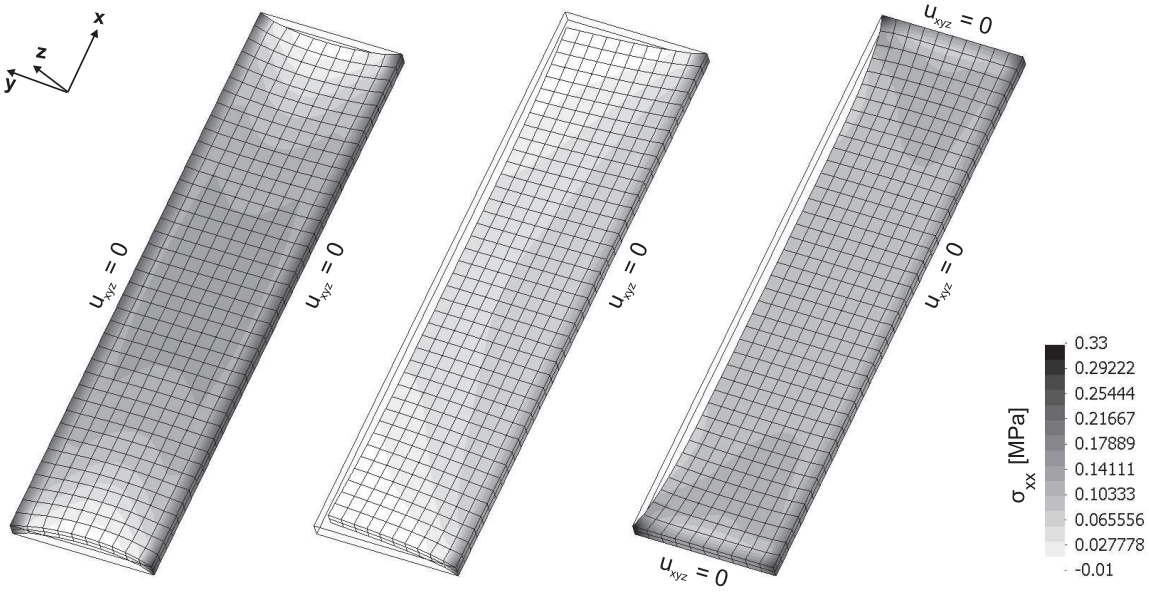

Fig. 7 Curing shrinkage of a thin three-dimensional plate subjected to three different bearing conditions, deformation (scaled by two) and Cauchy stress in x-direction after 20 seconds of curing. Elastic 21-chain curing model, extended by the multiplicative decomposition approach of Sec. 4.2. Model parameters: $[\mu_0, \mu_\infty, \kappa_\mu, N_0] = [0.0001$ MPa, 1.5 MPa, 0.25 s^{-1}, $2{\cdot}10^6]$

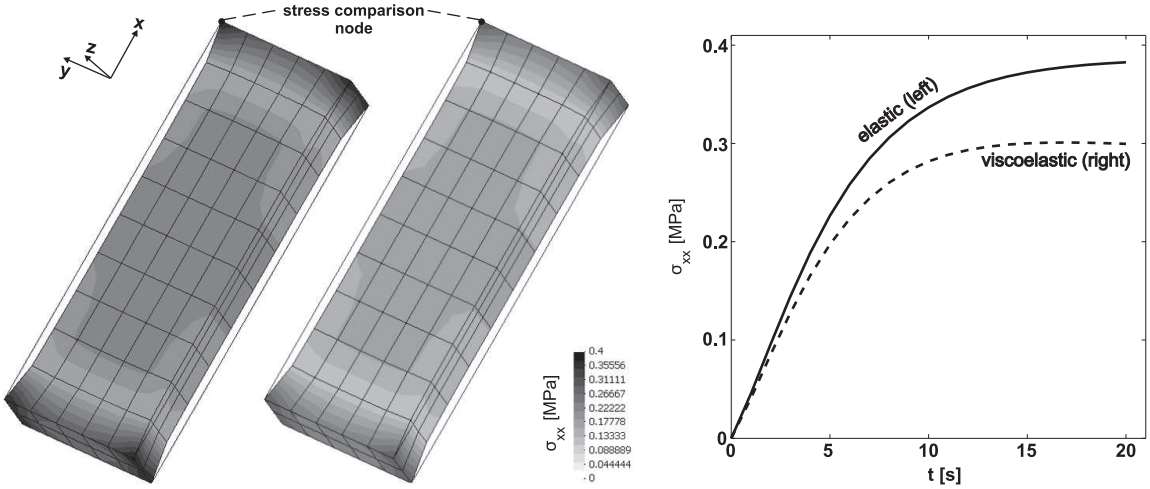

Fig. 8 Stress development in a block held at fixed length during curing, simulated with the viscoelastic 21-chain curing model together with the multiplicative decomposition approach for the volume shrinkage. Deformation (scaled by two) and Cauchy stress in x-direction after 20 seconds of curing for, **(left)**, the 'elastic' case with long ($T = 1500$ s) and constant relaxation time and, **(middle)**, the viscoelastic case with short and evolving relaxation time ($[T_0, T_\infty, \kappa_\tau] = [0.015$ s, 4.2 s, 0.25 $s^{-1}]$) time. Remaining model parameters: $[\mu_0, \mu_\infty, \kappa_\mu, N_0, \mu_v, \delta, \Delta t] = [0.0001$ MPa, 2.0 MPa, 0.25 s^{-1}, $2{\cdot}10^6$, 10.5 MPa, 1.5, 1 s]. Comparison of stress over time for the top left node **(right)**.

5.3.3 Curing shrinkage and viscoelasticity

The shrinkage phenomenon is of particular interest for viscoelastic materials that are able to decrease the arising stresses via relaxation already during curing – which would be the case for a majority of polymer materials. To demonstrate the behaviour if these reverse processes are active simultaneously we resort to the block example from Sec. 5.3.1 and compare elastic and viscoelastic simulations. By applying the viscoelastic 21-chain curing model with multiplicative decomposition shrinkage, 'elastic' behaviour is mimicked by choosing a constant and, in view of the curing process duration, infinite relaxation time while real 'viscoelastic' behaviour allowing for significant relaxation already during curing is realised with parameters similar to those from Fig. 5. The decrease of shrinkage induced residual stresses can be of remarkable magnitude, as is indicated by both the contour plots and the dispersing stress curves in Fig. 8.

6 Conclusion and outlook

Extending the previous part of this contribution, phenomenological and micro-mechanically based material models for the finite strain simulation of viscoelastic polymers that undergo curing processes and volume shrinkage have been proposed. The governing constitutive equations and the tangent operators are derived and the numerical realisation within the finite element framework is sketched. The numerical examples demonstrate that the developed models are suitable to correctly reproduce the relevant phenomena. Further extensions considering effects like exothermal reactions, thermoelastic coupling and elastoplastic material behaviour will be subject of forthcoming research.

Acknowledgements Financial support by the German Research Foundation (DFG) within the collaborative project PAK 108 is gratefully acknowledged.

References

1. M. Hossain, G. Possart, P. Steinmann (2009) A finite strain framework for the simulation of polymer curing. Part I: elasticity. Computational Mechanics 44 (5):621-630
2. M. Hossain, G. Possart, P. Steinmann (2009) A small-strain model to simulate the curing of thermosets. Computational Mechanics 43(6):769-779
3. C. Miehe, S. Göktepe (2005) A micro-macro approach to rubber-like materials: Part-II. The micro-sphere model of finite rubber viscoelasticity. Journal of the Mechanics and Physics of Solids 53:2231-2258
4. J.C. Simo,C. Miehe (1992) Associative coupled thermoplasticity at finite strains. Computer Methods in Applied Mechanics and Engineering 98:41-104
5. S. Göktepe (2007) Micro-macro approaches to rubbery and glassy polymers: Predictive micromechanically-based models and simulations. PhD Thesis, University of Stuttgart, Germany
6. S. Reese, S. Govindjee (1998) A theory of finite viscoelasticity and numerical aspects. International Journal of Solids and Structures 35:3455-3482
7. S. Govindjee, S. Reese (1997) A presentation and comparison of two large deformation viscoelasticity models. Journal of Engineering Materials and Technology 119:251-255
8. S. Reese (2003) A micromechanically motivated material model for the thermo-viscoelastic material behaviour of rubber-like materials. International Journal of Plasticity 19:909-940
9. B. Kleuter (2007) Generalized parameter identification for finite viscoelasticity. PhD Thesis, University of Kaiserslautern, Germany
10. B.D. Coleman, M.E. Gurtin (1967) Thermodynamics with internal state variables. Journal of Chemical Physics 47:597-613
11. M. Johlitz, H. Steeb, S. Diebels, A. Chatzouridou, J. Batal, W. Possart (2007) Experimental and theoretical investigation of nonlinear viscoelastic polyurethane systems. Journal of Material Science 42:9894-9904
12. J. Lubliner (1985) A model of rubber viscoelasticity. Mechanics Research Communications 12(2):93-99
13. N. Huber, C. Tsakmakis (2000) Finite deformation viscoelasticity laws. Mechanics of Materials 32:1-18
14. A.F.M.S. Amin, A. Lion, S. Sekita, Y. Okui (2006) Nonlinear dependence of viscosity in modeling the rate-dependent response of natural and high damping rubbers in compression and shear: Experimental identification and numerical verification. Internationl Journal of Plasticity 22:1610-1667
15. W. Kuhn, F. Grün (1942) Beziehungen zwischen elastischen Konstanten und Dehnungsdoppelbrechung hochelastischer Stoffe. Kolloid-Zeitschrift 101:248-271
16. J.S. Bergström, M.C. Boyce (1998) Constitutive model of the large-strain time-dependent behaviour of elastomers. Journal of the Mechanics and Physics of solids 46:931-954
17. M. Kiasat (200) Curing shrinkage and residual stresses in viscoelastic thermosetting resins and composites. PhD Thesis, TU Delft, Netherlands
18. A. Lion, P. Höfer (2007) On the phenomenological representation of curing phenomena in continuum mechanics. Archive of Mechanics 59:59-89
19. G. Himpel (2008) Computational modeling of biomechanical phenomena - remodeling, growth and reorientation. PhD Thesis, University of Kaiserslautern, Germany
20. J. Retka, P. Höfer (2007) Numerische Simulation aushärtender Klebstoffe. Diploma Thesis, Universität der Bundeswehr München

A finite strain framework for the simulation of polymer curing Part 2: viscoelasticity and shrinkage

M. Hossain, G. Possart and P. Steinmann

For both the computer-aided development and the lifetime prediction of polymer components it is absolutely necessary to simulate their production processes. To this end, constitutive models describing all relevant phenomena (e.g. the changes in the mechanical material behaviour during and after the curing reaction, the kinetics of the reaction and the chemical shrinkage) in combination with efficient finite element algorithms are needed. The current essay, denoted as part 2, belongs to a series of a total of three comprehensive papers which were provided by the authors. In part 2, the elastic approach of part 1 is extended in order to take viscoelastic phenomena and chemical shrinkage into account. In the paper, two different approaches to consider the chemical shrinkage are introduced as well as two different models for the elastic and viscoelastic parts of the free energy. Each model was implemented into a FEM code and the corresponding update algorithms and tangent operators are derived. The stress responses of the different models are visualized using finite element simulations. The manuscript is recommended for publication in Computational Mechanics but the following remarks should be considered.

1. On page 2, the authors note that the thermodynamical consistency of the model defined by eq. (1) has been demonstrated in part 1. Normally, such a proof requires formulating a free energy function. When the time-dependent fourth order tensor $\mathbb{C}(t) = 4\frac{\partial^2 \psi}{\partial \boldsymbol{C}^2}$ is derived on the basis of a free energy function ψ which is the relation between this free energy and that of eq. (1)?

Answer: GP

2. The difference between the free energy function ψ_{eq} in eq. (4) or eq. (13) and the function ψ used to calculate the tensor $\mathbb{C}(t)$ should be clarified. In order to avoid complications, it is proposed to take the choice of different symbols, for example $\mathbb{C}(t) = 4\frac{\partial^2 \Psi}{\partial \boldsymbol{C}^2}$ instead of $\mathbb{C}(t) = 4\frac{\partial^2 \psi}{\partial \boldsymbol{C}^2}$.The symbol ψ_{eq} could then be used for the free energy belonging to eq. (1). The expressions for ψ_{eq} in eq. (13) or eq. (29) are used to calculate the tensor $\mathbb{C}(t)$ and should not be denoted as ψ_{eq}.

Answer: GP

3.The authors note that eq. (21) is the linearized flow rule for the inelastic Cauchy-Green tensor - a reference to a paper by Reese and Govindjee is given. In order to improve the understanding, the fundamental form of the nonlinear flow rule should be introduced and the linearization procedure should be sketched. In addition, a motivation for the linearization should be given. Reese and Govindjee as well as other authors developed update schemes for nonlinear flow rules.

Answer: MH

From the Coleman & Noll argument, it can be implied from equation (10) that the evolution equation for the internal viscous part of the deformation must satisfy the remainder or dissipation inequality

$$-\frac{\partial \Psi_{neq}}{\partial \boldsymbol{C}_e} : \frac{\partial \boldsymbol{C}_e}{\partial \boldsymbol{F}_v} : \dot{\boldsymbol{F}}_v \geq 0, \tag{48}$$

which also can be rewritten in the form below exploiting the symmetry properties,

$$-2\frac{\partial \Psi_{neq}}{\partial \boldsymbol{C}_e} : (\boldsymbol{C}_e \cdot \boldsymbol{l}_v) \geq 0. \tag{49}$$

In equation (49), $\boldsymbol{l}_v = \dot{\boldsymbol{F}}_v \cdot \boldsymbol{F}_v^{-1}$ is the viscous part of the spatial velocity gradient $\boldsymbol{l} = \dot{\boldsymbol{F}} \cdot \boldsymbol{F}^{-1}$. Again using the symmetry property and assuming that Ψ_{neq} is an isotropic function of $\boldsymbol{C}_e$, the residual inequality can be expressible as

$$-\boldsymbol{\tau}_{neq} : \frac{1}{2}(\mathscr{L}_v \boldsymbol{b}_e) \cdot \boldsymbol{b}_e^{-1} \geq 0, \tag{50}$$

where $\mathscr{L}_v \boldsymbol{b}_e$ stands for the Lie derivative of the contravariant tensor $\boldsymbol{b}_e = \boldsymbol{F}_e \cdot \boldsymbol{F}_e^t$ and $\tau_{neq} = 2\boldsymbol{F}_e \cdot \frac{\partial \Psi_{neq}}{\partial \boldsymbol{C}_e} \cdot \boldsymbol{F}_e^{-1}$. Within the context of finite elastoplasticity, the dissipation inequality (50) is well-known; see e.g., Simo & Miehe [4]. A sufficient condition fulfilling (50) is to make it a positive definite quadratic form. This natural choice gives evolution equation

$$-\frac{1}{2}\mathscr{L}_v \boldsymbol{b}_e \cdot \boldsymbol{b}_e^{-1} = \mathscr{V}^{-1} : \boldsymbol{\tau}_{neq}, \tag{51}$$

where $\mathscr{V}^{-1}$ is a positive definite rank four isotropic tensor to satisfy (50), see Reese & Govindjee [6] for further elaboration. Since equation (51) is applicable for large perturbations away from thermodynamic equilibrium, one linearization step is followed to it, e.g. linearize about/around thermodynamic equilibrium, i.e. $\boldsymbol{b}_e \approx \boldsymbol{I}$ which is still valid for large deformation case but is restricted to small perturbations away from thermodynamic equilibrium. Combining all these facts, the linearized evolution equation close to the thermodynamic equilibrium system yields

$$-\frac{1}{2}(\mathscr{L}_v \boldsymbol{b}_e \cdot \boldsymbol{b}_e^{-1})_{lin} = \frac{1}{2T}(\boldsymbol{b}_e - \boldsymbol{I}), \tag{52}$$

where T is the relaxation time. Furthermore, using the definition of Lie derivative, equation (52) can be simplified as

$$\dot{\boldsymbol{C}}_v = T^{-1}\left[\boldsymbol{C} - \boldsymbol{C}_v\right]. \tag{53}$$

which was used as finite linear viscoelasticity evolution rule in some literature, e.g. in Lubliner [12], Reese [8], Johlitz et al. [11]. The main motivation for using the linearized evolution equation (53) is to make the local update of the evolution formulation as simple as possible, i.e. the local update for the internal variable ($\boldsymbol{C}_v$) can be performed using an Euler-forward/backward integration scheme which avoids complicated iteration in the Gauss-point level that is normally done by some well-known iterative solvers, e.g. Newton-Raphson method.

4.Since the use of differences of Cauchy-Green tensors is uncommon in material theory, a more detailed discussion of the approach defined by eq. (40) should be introduced in the revised version. Is this approach compatible with the Clausius Duhem inequality? The authors also applied a multiplicative formulation to describe the chemical shrinkage. Are their any differences?

Answer: MH

The main framework for finite strain elastic curing (2) is thermodynamically consistent as proved in Hossain et al. [1]. The shrinkage formulation (40) is nothing but the replacement of strain tensor $\boldsymbol{C}$ by another effective strain tensor ($\boldsymbol{C}_n - C_s\boldsymbol{I}$) and this formulation is not thermodynamically consistent since stress exists even in the absence of external (mechanical) loading. It might be the answer that this extra potential is balanced somehow by the heat generation of the exothermal reactions during curing process. Two approaches for modelling the shrinkage phenomenon within our main curing framework are absolutely different. Predefined function approach is applied in the main framework of the stress update equation considering that material responds isotropically and negative strain are substracted only in the orthogonal directions. On the other hand, the multiplicative deformation approach is applied in the main ingredient of the strain tensor, i.e. by decomposing the deformation gradient into the stress-producing mechanical part and the volume-reduction shrinkage part.

5.Different energy functions for the elastic and inelastic parts of the constitutive model as well as different approaches for the shrinkage model are proposed. Since the simulated responses look very similar, the resulting differences should be discussed in more detail. The reader expects a recommendation.

Answer: MH

If one wants to use the model for shrinkage with the pre-defined shrinkage function, one has to determine the material parameters once for the shrinkage function, another time for the degree of cure while in case of the multiplicative decompostion approach for the shrinkage modelling, only the material parameters for the degree of cure (α) have to be determined once. Additonally, it can be stated here, the multiplicative decomposition approach is well-known and its theoretical background is also explicitly elaborated and well-established, e.g. in viscoelasticity, viscoplasticity, see in the literature . But major advantage of the pre-defined approach is that, it is easy to implement and straight-forward compared to the multiplicative decomposition approach.